Journal of Rock Mechanics and Geotechnical Engineering 14 (2022) 909–921

Contents lists available at ScienceDirect

Journal of Rock Mechanics and Geotechnical Engineering

journal homepage: www.jrmge.cn

Full Length Article

Use of recycled gypsum in the cement-based stabilization of very soft clays and its micro-mechanism

Jun Wu [a], Li Liu [a,b], Yongfeng Deng [a,*], Guoping Zhang [b], Annan Zhou [c], Henglin Xiao [d]

[a] Institute of Geotechnical Engineering, School of Transportation, Southeast University, Nanjing, 211189, China
[b] Department of Civil and Environmental Engineering, University of Massachusetts Amherst, Amherst, MA, 01003, USA
[c] Civil and Infrastructure Engineering, School of Engineering, Royal Melbourne Institute of Technology (RMIT), Melbourne, VIC, 3001, Australia
[d] Department of Civil Engineering, Hubei University of Technology, Wuhan, 430068, China

ARTICLE INFO

Article history:
Received 25 April 2021
Received in revised form
19 August 2021
Accepted 18 October 2021
Available online 25 November 2021

Keywords:
Cement-based stabilized clay (CBSC)
Cement clinker
Gypsum
Ettringite
Unconfined compressive strength (UCS)
Micro-mechanism

ABSTRACT

This paper presents an experimental study and micro-mechanism discussion on gypsum role in the mechanical improvements of cement-based stabilized clay (CBSC). A soft marine clay at two initial water contents (i.e. 50% and 70%) was treated by reconstituted cementitious binders with varying gypsum to clinker (G/C) ratios and added metakaolin to facilitate the formation of ettringite, followed by the measurements of final water contents, dry densities and strengths in accordance with ASTM standards as well as microstructure by mercury intrusion porosimetry (MIP) and scanning electron microscopy (SEM). Results reveal that the gypsum fraction has a significant influence on the index and mechanical properties of the CBSC, and there exists a threshold of the G/C ratio, which is 10% and 15% for clays with 50% and 70% initial water contents, respectively. Beyond which adding excessive gypsum cannot improve the strength further, eliminating the beneficial role. At these thresholds of the G/C ratio, the unconfined compressive strength (UCS) values for clays with 50% and 70% initial water contents are 1.74 MPa and 1.53 MPa at 60 d of curing, respectively. Microstructure characterization shows that, besides the common cementation-induced strengthening, newly formed ettringite also acts as significant pore infills, and the associated remarkable volumetric expansion is responsible, and may be the primary factor, for the beneficial strength gain due to the added gypsum. Moreover, pore-filling ettringite also leads to the conversion of relatively large inter-aggregate to smaller intra-aggregate pores, thereby causing a more homogeneous matrix or solid skeleton with higher strength. Overall, added gypsum plays a vital beneficial role in the strength development of the CBSC, especially for very soft clays.

1. Introduction

Rapid growing industrial and residential settlements in the coastal areas provide an impetus for the demand on land reclamation, ground improvement, and soil stabilization for soft alluvial, estuarine, and marine clays, usually characterized by high water content, high compressibility, and low undrained shear strength. One economical, widely implemented ground improvement technique, particularly developed for the treatment of soft, weak, incompetent coastal clayey sediments, is stabilization by mixing cement as additives. In recent decades, many studies have been performed on the performance of cement-based stabilized clays (CBSC), owing to the highly diverse and complex nature of these natural soft soils (Tremblay et al., 2001; Tsuchida and Tang, 2015; Liu et al., 2019; Oluwatuyi et al., 2019).

Despite the complex nature and diverse applications of ordinary Portland cement (OPC), in general, its constituents are primarily designed for such applications as grouts and pastes (i.e. cement and water mixture), mortars (i.e. mixtures of cement, water and sand), and concretes (i.e. mixtures of cement, water, sand and gravel). However, the threshold fractions of some minor constituents such as non-hydrated free lime (f-CaO), MgO, SO_3 and Cl^-, are often limited to minimize or even eliminate the internal structural disruption and damage induced by the expansion of certain free oxides (e.g. CaO and MgO) and hydrated ettringite, as well as the corrosion of Cl^- on the reinforcing steel rebars used in concretes (Taylor, 1997). For instance, the gypsum fraction is usually

* Corresponding author.
E-mail address: noden@seu.edu.cn (Y. Deng).
Peer review under responsibility of Institute of Rock and Soil Mechanics, Chinese Academy of Sciences.

https://doi.org/10.1016/j.jrmge.2021.10.002

stipulated to be less than 4% in OPC, according to some standards such as ASTM C150-21 (2021) and BS EN197-1 (2011). Indeed, these standards apply to the Portland cement-based pastes, mortars, and concretes, and its requirement for a low gypsum fraction is due to the consideration of the uniform and dense structure of these hardened cement products that hence can accommodate little or are prone to damage by aforementioned internal expansion and resulting swelling stresses.

For the general cement-based soil stabilization, OPC mainly plays a cementitious role in bonding together solid particulates, including fine-grained clay and silt particles, coarse-grained sand particles, and secondary clay aggregates, through the hydration of reactive cement constituents and alkali-activated pozzolanic reactions. After that, a series of complex chemical reactions with different rates takes place among the clinker, gypsum, and water as well as CO_2 from the atmosphere to form various hydration products, including calcium hydroxide (CH), calcium silicate hydrates (C–S–H), calcium aluminate hydrate (C-A-H), ettringite, calcium carbonates ($CaCO_3$), and tetracalcium aluminate-ferrite hydrates (AFm) (Gerry et al., 2011). However, since soft clays usually have extremely high water contents and sometimes high organic matter contents, their high porosity may remain even after stabilization by OPC that mainly functions by providing cementation among soil particles. In that sense, it can be speculated that the limited ettringite hydrated from gypsum may not always induce devastating effects such as swelling and cracking of the CBSC. In the contrary, the expansion due to the newly formed ettringites is expected to significantly reduce the voids and thereby densify the stabilized clay, which plays a primary role in the strength gain and pertinent microstructural change of the CBSC. Nevertheless, the current design guidelines fail to recognize this essential issue. Hence, when further strength improvement is desired, an increase in the Portland cement content and the inclusion of supplementary cementitious materials (SCMs) rather than adjusting the gypsum dosage are the commonly accepted methods at present (Eyo et al., 2020; Oluwatuyi et al., 2020), which is more costly and detrimental in terms of resource conservation and economical effects.

Quite a few attempts have been made on the efficient reuse of gypsum-based wastes or by-products to reduce the carbon footprint of soil improvement (e.g. phosphogypsum, flurogypsum, citrogypsum, desulphogypsum, borogypsum, and flue gas desulfurization (FGD) gypsum) to ameliorate problematic soils, such as loess (Zhao et al., 2019; Gu and Chen, 2020), expansive clays (Yilmaz and Civelekoglu, 2009), and swelling bentonites (Ahmed and El Naggar, 2016), among others. Such waste-based alternative binders are seen as a sustainable solution to soil stabilization by reducing the usage of OPC whose production involves greenhouse gas emission, a significant factor for global climate change. Despite the observed significant improvement in the behavior and performance of the gypsum-treated soils, the underlying mechanisms of gypsum-based stabilization of soils, in particular soft clays, remain unknown or fragmental and have yet to be uncovered. Additionally, an important consideration is that the OPC itself contains various amounts (mostly less than 4%) of gypsum to retard the setting time (Suarez et al., 2016), which would inevitably compromise the accuracy for determining the dosages of gypsum as a supplementary cementitious binder. Therefore, the role of gypsum in the CBSC should be systematically investigated to facilitate the establishment of gypsum dosage benchmark within the cementitious binders particularly designed for soft clay stabilizations.

With the incorporation of gypsum, a hydrous calcium aluminium sulfate mineral ($Ca_6[Al(OH)_6]_2(SO_4)_3{\cdot}26H_2O$), also termed ettringite, is usually observed in the CBSC after hydration (Puppala et al., 2004; Tang et al., 2015; Pu et al., 2021), which can be schematically formulated by

$$3CaO\cdot Al_2O_3+3(CaSO_4\cdot 2H_2O)+26H_2O \rightarrow Ca_6\left[Al(OH)_6\right]_2(SO_4)_3\cdot 26H_2O \quad (1)$$

More importantly, the amount of ettringite-induced swelling can cause more than a 100% volumetric expansion (Taylor, 1997; Zhang et al., 2015), which can prominently influence or reduce the porosity of the CBSC, as discussed earlier. In addition, it is worth noting that the alumina phase also plays a significant role in the formation of ettringite, as shown in Eq. (1). However, this component is scarce in gypsum, which limits its reuse efficiency. As such, the metakaolin, a kind of cementitious alternative by calcinating pure kaolinite at a temperature of 500 °C–550 °C that contains both amorphous SiO_2 and Al_2O_3, can be just added to supply the alumina phase to gypsum, promoting the formation of ettringite (Deng et al., 2015; Wu et al., 2019a).

In this paper, the effect of gypsum fraction on the mechanical behavior of the CBSC is presented and discussed, based on the results of a series of unconfined compression testing performed on the CBSC with different gypsum to clinker (G/C) ratios. The objective of this study is to validate the feasibility of re-establishing a design guideline for cementitious binders that are only applicable to soft clays by adjusting the gypsum fractions, which can function as a beneficial role. This is an innovative and cost-effective method for the treatment of soft clays as well as the beneficial reuse of industrial gypsum wastes, resulting in dual benefits.

2. Materials and methods

2.1. Materials

The studied soil sample was recovered from Fuzhou, a coastal city in southeast China, at depths of >1 m below the ground surface. Immediately after extraction from the ground, the sample was completely sealed in a polyethene bag and wrapped by duct tape to avoid moisture loss during transportation and storage. It was a type of Quaternary marine sediments with very high water content, high compressibility, and high sensitivity, resulting in a high porosity and low strength. Its basic properties are presented in Table 1 and Fig. 1 following relevant ASTM standards (ASTM D854-14, 2014; ASTM D2487-17, 2017).

Two cementitious admixtures, a clinker produced in a Portland cement plant, Fuzhou, China, and a metakaolin manufactured by BASF, Germany, were adopted in this study for soft clay improvement. Their chemical compositions are presented in Table 2. The former was made by firing limestone ($CaCO_3$) in conjunction with clay and ferric oxide (Fe_2O_3) powder in a cement kiln at about 1450 °C, followed by grinding the sintered product to a fineness of 350 m^2/kg, and the resulting powder or the clinker had a Ca/Si

Table 1
Basic physical and index properties of the studied soft marine clay.

Property	Value
Natural water content, w_0 (%)	58.2
Specific density, G_s	2.71
Total density, ρ (g/cm^3)	1.7
Initial void ratio, e_0	1.69
Liquid limit, *LL* (%)	46.2
Plastic limit, *PL* (%)	25.3
Plasticity index, *PI* (%)	20.9
Sand fraction (>0.075 mm) (%)	1.2
Silt fraction (0.002–0.075 mm) (%)	49.1
Clay fraction (<0.002 mm) (%)	49.7
USCS classification	Lean clay (CL)

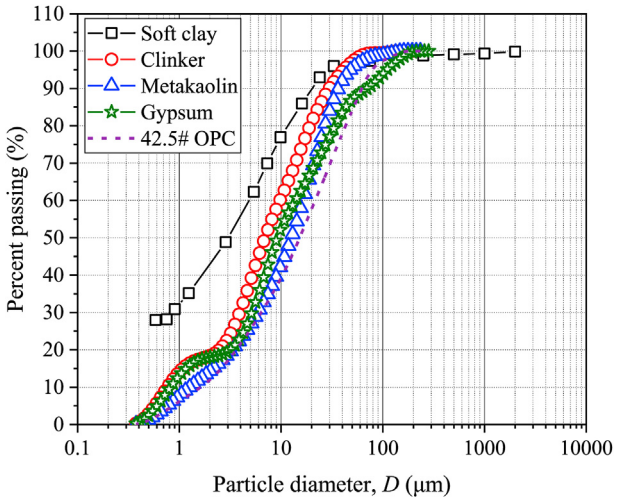

Fig. 1. Grain size distribution curves of the studied soft clay, clinker, metakaolin, gypsum and the referential 42.5# OPC.

molar ratio of 2.7 and a MgO content of <3%. The aforementioned properties of the clinker were similar to those of OPC and met the requirements of the European Cement Standard (BS EN197-1, 2011). The latter, resulting from the calcination of kaolin clays, consisted predominantly of amorphous SiO_2 and Al_2O_3 as the reactive phases accounting for a total content of approximately 92%, which can be activated by alkali and alkaline solutions via pozzolanic reactions, resulting in the formation of extra cementation that improves the counterpart caused by clinker hydration (Justice and Kurtis, 2007; Kim et al., 2007). The particle size distribution curves of the clinker and metakaolin are also shown in Fig. 1. The clinker has a median particle size (D_{50}), coefficient of uniformity (C_U), and coefficient of curvature (C_C) of 7.049 μm, 12.79 and 1.96, respectively, while those for the metakaolin are 12.625 μm, 13.31 and 1.73, respectively.

In addition, an FGD gypsum, primarily composed of calcium sulfate dihydrate ($CaSO_4 \cdot 2H_2O$), was selected as a special additive for soft clay improvement to bring multi-faceted engineering, economic, and ecological benefits such as waste minimization, reuse, and management (Xu et al., 2017). The FGD gypsum sample was obtained from a local power plant that employed a limestone-gypsum desulfurization process in Fujian Province, China. Its chemical compositions (Table 2) determined by X-ray fluorescence (XRF) showed that the gypsum sample generally consisted of more than 40% SO_3, while its particle size distribution curve (Fig. 1) indicated that the median particle size (D_{50}), coefficient of uniformity (C_U), and coefficient of curvature (C_C) were 9.156 μm, 17.26 and 2.4, respectively. Note that the particle size distributions of the adopted clinker, metakaolin and gypsum were similar to that of 42.5# OPC.

2.2. Sample preparation

The mix designs for the clay stabilization experiments are tabulated in Table 3. The collected marine clay sample was first oven-dried at 50 °C as per ASTM D1632-17 (2017) to avoid over-drying or over-dehydration of certain minerals, followed by crushing the dried material with a rubber hammer and then sieving the crushed soil through a No. 10 (i.e. equivalent to an opening sieve dimension of 2 mm) mesh to remove coarser sand and gravel particles as well as other coarse impurities (e.g. undecomposed roots or woody organic matter). Then distilled water was added to the dry soil at two pre-designed water contents, 50% and 70%, or approximately 1.1 and 1.5 times the *LL*, respectively, to simulate the initial in situ consistency of the soft clays to be stabilized by the clinker, followed by curing in a sealed container for more than 24 h to reach moisture homogenization and equilibrium. Finally, the cementitious admixtures consisting of clinker, gypsum and metakaolin were consecutively added to the above prepared wet soil at a clinker to dry soil ratio of 12%, G/C ratio of 0%, 5%, 10%, 15% and 20%, and a metakaolin to clinker ratio of 25%. Noteworthy is that the G/C ratio was varied to examine and verify its potentially beneficial role in soft clay improvement, but the metakaolin to cement ratio remained constant at 25% based on previous research (Zhang et al., 2014; Wu et al., 2016, 2019b). Also, the total contents of the selected binders (i.e. clinker, gypsum and metakaolin mixture) in the mix designs were close to those typical values (i.e. usually ranging from 15% to 20%) recommended or adopted in most ground improvement projects in highway construction in China (Liu et al., 2019).

The above mixture consisting of wet clay, clinker, gypsum and metakaolin was blended in an electric mixer for 5–10 min at a speed of 60–120 revolutions per minute to achieve a homogeneously mixed soil paste and then transferred into cylindrical, two halves-split, polyvinyl chloride (PVC) molds with an inner diameter and height of 46 mm and 100 mm, respectively. The soil paste-filled molds were vibrated for compaction to remove entrapped air bubbles and improve uniformity. Three replicate specimens were prepared for each mix design to check the reproducibility and to obtain representative mechanical properties averaged from multiple specimens. After the initial 48 h curing, they were carefully demolded, and their dimensions and weights were tracked for quality control, only those three replicate specimens with the deviations in weight and dimension within ±0.5% and ±0.5 mm were used for subsequent mechanical testing, while those failing to meet these requirements were discarded and the above procedures were repeated to prepare a new set of specimens. Each of these qualified specimens

Table 3
Summary of mix designs for the clay stabilization experiments.

Sample ID	G/C ratio (%)	Content of binder (%)			
		Clinker	Gypsum	Metakaolin	Water
0G/C–50W	0	12	0	3	50
5G/C–50W	5	12	0.6	3	50
10G/C–50W	10	12	1.2	3	50
15G/C–50W	15	12	1.8	3	50
20G/C–50W	20	12	2.4	3	50
0G/C–70W	0	12	0	3	70
5G/C–70W	5	12	0.6	3	70
10G/C–70W	10	12	1.2	3	70
15G/C–70W	15	12	1.8	3	70
20G/C–70W	20	12	2.4	3	70

Note: Sample ID notation such as 10G/C–50W represents a sample prepared with a G/C ratio of 10% and an initial water content of 50%.

Table 2
Chemical compositions (%) of clinker, metakaolin and gypsum.

Composition	SiO_2	Al_2O_3	CaO	Fe_2O_3	MgO	Na_2O	SO_3	K_2O	Loss on ignition	Total
Clinker	22.1	6.5	55.8	3.2	2.6	0.2	4.1	0.3	4.9	99.7
Metakaolin	52	40	1	2.5	0.8	0.5			3.1	99.9
Gypsum	2.1	1.4	33.8	0.4			41.7		15.4	94.8

was wrapped, but without complete air-tight sealing, in a polyethene bag and further cured in a standard curing room (relative humidity of 95% and temperature of (20 ± 2) °C) for additional 5 d, 12 d, 26 d and 58 d. Given the initial 48 h curing inside the split molds, the total curing durations for each mix design included 7 d, 14 d, 28 d and 60 d. Such a sample preparation procedure has been widely used in the laboratory for the experimental study of soft clay stabilization (Horpibulsuk et al., 2004; Wu et al., 2019b).

2.3. Mechanical testing

Upon curing to the predetermined duration (i.e. 7 d, 14 d, 28 d and 60 d), unconfined compressive strength (UCS) measurements were conducted following ASTM D2166M-16 (2016). Before testing, the dimensions and weights of the specimens were measured. An automated loading machine with load and displacement resolutions of 0.1 N and 0.01 mm, respectively was used to apply the load monotonically at a constant displacement rate of 1 mm/min until the specimen failed or the strain reached 15%. The vertical strain of the specimen was measured by a linear variable differential transducer (LVDT), and both the load cell and LVDT were connected to a data logger that was connected to a personal computer for data acquisition. Again, for quality control and data accuracy, the strength of each specimen from the three replicates prepared under the same conditions should not differ by more than 10% from the averaged value. Otherwise, the results were discarded and new specimens were prepared. In the end, the water content of each specimen was measured, and the dry density was calculated.

2.4. Microstructural characterization

To analyze the microstructure, fragments selected from the specimens that failed by the UCS testing were first lyophilized via freeze-drying, which involved immersion of the samples into liquid nitrogen with a temperature of −196 °C for instant freezing, followed by transfer to a XIANOU-18 N freeze-dryer (ATPIO Instrument Corp., China) in which the temperature and vacuum pressure were kept at −55 °C and 0.04 Pa, respectively for sublimation until the sample was completely dried. Such representative dry samples were then analyzed by mercury intrusion porosimetry (MIP) and scanning electron microscopy (SEM) following previous studies (Wu et al., 2019a; Deng et al., 2020; Eyo et al., 2021).

The MIP was conducted in an Autopore IV 9500 mercury intrusion porosimeter (Micromeritics Instrument Corp., USA) that operates at pressures ranging from 3.7 kPa to 241.1 MPa.

To achieve an in-depth understanding of the characteristics of pore size distribution (PSD) curves, statistical deconvolution was adopted to identify and analyze whether the PSD curves of these samples exhibited unimodal, bimodal, or even multimodal peaks. In a typical one-dimensional analysis, a log-normal distribution function was assumed for each characteristic pore size, defined as a random variable d, with a mean and standard deviation of m and s, respectively. As such, the overall probability density function (PDF) of the pore sizes of the porous soil mass that consisted possibly of multiple characteristic pore sizes was the summation of each PDF for each pertinent characteristic pore size, as expressed in the following equation:

$$P(d) = \sum_{i=1}^{n} P_i(d) = \sum_{i=1}^{n} a_i \frac{1}{\sqrt{2\pi}\sigma_i} e^{-\left[(\log_{10} d - \log_{10}\mu_i)^2 / (2\sigma_i^2)\right]} \quad (2)$$

where n is the total number of characteristic pore sizes, each of which corresponded to a peak in the pore size PDF curves on a logarithmic scale (e.g. $n = 1$ and 2 for the unimodal and bimodal distributions, corresponding to one and two characteristic pore sizes, respectively); a_i is the fraction of the pore volume for the i-th characteristic pore size per unit mass of the dry soil (mL/g); σ_i is the standard deviation of the logarithmic pore size d; and μ_i is the mean of the i-th characteristic pore size. More details on the PDF-based deconvolution of a mixture's statistical distribution for unimodal and bimodal PSD curves can be found in the literature (Du et al., 2014; Luo et al., 2020).

Microstructure imaging and observation were performed in a SU3500 scanning electron microscope (HITACHI High-tech Corp., Japan) on the freeze-dried samples, which were sputter-coated with a gold layer of 20–30 nm in thickness on their fresh surface to avoid the potential charge effect.

3. Analyses of results

3.1. Physical properties

Fig. 2 shows the final water contents and final dry densities of all specimens prepared at two initial water contents of 50% and 70% and different G/C ratios after 60 d of curing. It can be observed that the final water content (Fig. 2a) decreases with increasing G/C ratio, while the final dry density (Fig. 2b) shows an opposite trend. Also,

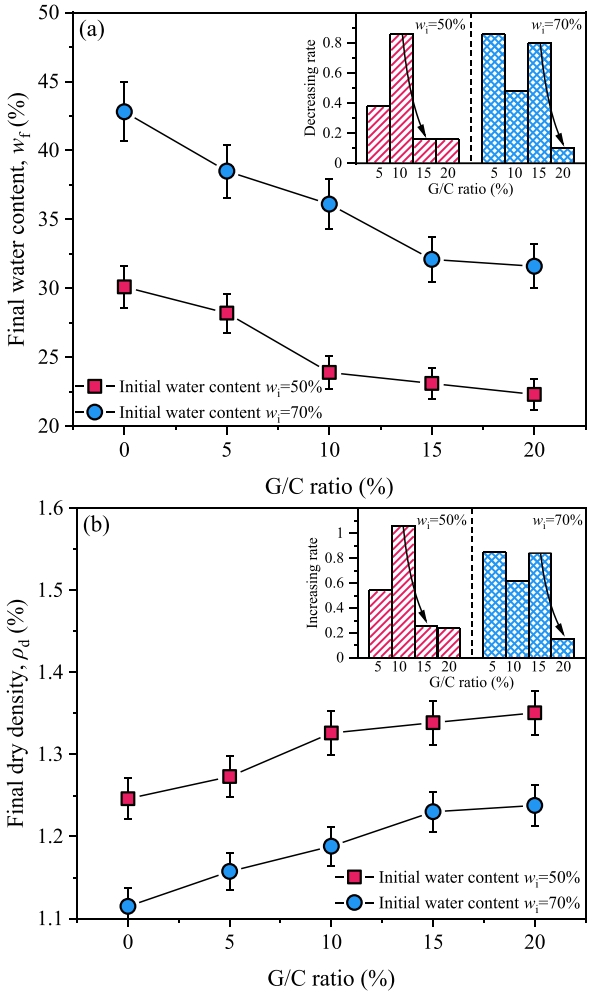

Fig. 2. Evolution of the final water content and dry density of the CBSC samples with varying the G/C ratios at two different initial water contents after 60 d of curing: (a) Final water content, and (b) Final dry density.

the final water content and final dry density of the treated specimens significantly depend on the initial water content. For example, for the specimen prepared with an initial water content of 50% and a G/C ratio of 20%, the final water content decreases from 30.1% to 22.3% after curing for 60 d (Fig. 2a) and the corresponding final dry density is 1.35 g/cm^3 (Fig. 2b). When the initial water content increases to 70%, the addition of the same dosage of cementitious binders (i.e. including the admixture of clinker, gypsum and metakaolin) reduces the final water content from 42.8% to 31.6% (Fig. 2a) and the corresponding final dry density is 1.24 g/cm^3 after curing for 60 d (Fig. 2b). The decrease in water content can be attributed to two major reasons: (1) the increased fraction of the solid phase by adding cementitious binders to the soft clay, and (2) the consumption and incorporation of water by chemical reactions of the cementitious binders (e.g. hydration and pozzolanic reactions of the clinker, gypsum and metakaolin, as further discussed later). The higher the dosage of added cementitious binders, the more the water that is involved in chemical reactions. However, the final dry density of the treated soft clays has an opposite trend, which increases with the content of cementitious binders, because the total solid content in the mixture increases with increasing fraction of cementitious binders. Higher content of the constituent cementitious binders implies more intensive and extensive reactions with the soft clay to produce a denser product in which more pores among the soil particles are filled such that the internal packing of particles is denser than that of the untreated soft clay. It can be seen that the final water content and final dry density curves at different G/C ratios are consistent with each other. In essence, cementitious binders and clay particles have undergone gelation reactions that generate interparticle cementation or pore infills, leading to a decrease in water content and an increase in dry density. Additionally, it is worth emphasizing that the rate of water content decrease and the rate of dry density increase, defined as the slopes of these curves shown in Fig. 2, both decrease with increasing G/C ratio. The underlying reason is most possibly because the growing impetus of ettringite is impeded or hindered by the limited pore space in the densely packed soil matrix, since the formation of ettringite results in significant volumetric expansion caused by the incorporation of 26 crystallization water molecules into its structure (Eq. (1)).

It is worth emphasizing that there should exist a critical threshold of the G/C ratio, which serves as a transition point. Before such a transition point, the final water content versus the G/C ratio curves tend to decrease at a higher rate, and thereafter decrease slowly with further increasing the G/C ratio. Meanwhile, the final dry density curves show an increasing trend in a similar manner. Such a threshold of the G/C ratio closely depends upon the initial water content, i.e. a G/C ratio of 10% as the threshold for specimens with a 50% initial water content whilst 15% for those with a 70% initial water content. The reason is most likely the non-negligible but beneficial effect of ettringite generated by the added gypsum, as discussed later.

3.2. Mechanical properties

3.2.1. General stress-strain relationships

Fig. 3 presents the typical stress-strain curves of the CBSC with varying G/C ratios at two initial water contents after 60 d of curing. The stabilized samples exhibit a distinct peak strength at an axial failure strain (ε_f) of approximately 1.49%–2.86% and 1.61%–3.13% at initial water contents of 50% and 70%, respectively, followed by significant strain-softening as indicated by a sharp decrease in the axial stress. The stiffness of the samples with the initial water contents of 50% and 70% is both positively correlated to the G/C ratio. For example, the ε_f values corresponding to the G/C ratios of

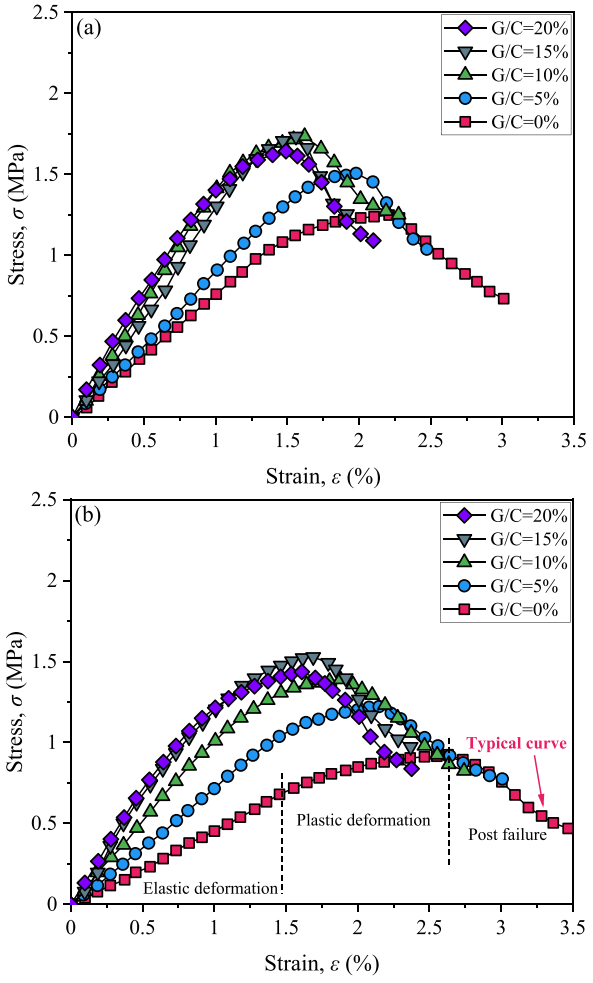

Fig. 3. Axial stress-strain curves of the CBSC with varying G/C ratios at two initial water contents after 60 d of curing: (a) 50% initial water content, and (b) 70% initial water content.

0%, 5%, 10%, 15% and 20% are respectively 2.21%, 1.98%, 1.62%, 1.56% and 1.49% for those samples with a 50% initial water content, while the corresponding peak strengths are 1.25 MPa, 1.51 MPa, 1.74 MPa, 1.73 MPa and 1.64 MPa, respectively.

It is observed that the stress-strain behavior of the CBSC is significantly affected by the addition of gypsum as a special cementitious binder. The stress-strain curves for various G/C ratios (e.g. a typical curve as marked in Fig. 3b) can be divided into three stages: (1) purely elastic deformation stage: the axial stress approximately increases linearly with the axial strain; (2) elasto-plastic deformation stage: the axial stress increases nonlinearly with the axial strain, at a rate relatively slower than that at the first, linearly elastic stage, up to the point of the peak stress; and (3) post-failure stage: once the axial stress reaches the peak strength, it starts to decrease sharply with increasing axial strain, and the soil exhibits significant strain-softening at this post-failure stage.

3.2.2. Strength and stiffness

The improvement to the UCS as well as the secant modulus (E_{50}) of the CBSC can be defined based on the above stress-strain curves. The definition of E_{50} is consistent with that of Lee et al. (2005), which is expressed by the ratio of the axial stress at 50% of the UCS to the pertinent axial strain. Determination of E_{50}, ε_f and UCS is

important for bearing capacity and settlement analyses of foundations when the stabilized soils are used as a bearing stratum.

The temporal dependence of the UCS of the CBSC on the G/C ratio after 7 d, 28 d and 60 d of curing is shown in Fig. 4. The threshold of the G/C ratio is determined as the point on the UCS versus G/C ratio curves beyond which further addition of the gypsum or the increase in the G/C ratio does not improve the strength further. For example, the UCS of the specimens after 60 d of curing reaches the peak value at the G/C ratios of 10% and 15% for the initial water contents of 50% and 70%, respectively. After that, the UCS tends to stabilize or even decrease slightly with increasing G/C ratio, regardless of the initial water contents. This indicates that, at this threshold of the G/C ratio, the most effective improvement is achieved. Additionally, based on the 7-, 28- and 60-d UCS results, the strength increase rates, defined as $(UCS_{28d \text{ or } 60d} - UCS_{7d})/UCS_{7d}$, were calculated and are summarized in Fig. 4. The results indicate a decreasing trend of increase rate in strength with increasing curing durations at high G/C ratio, suggesting that the selection of the optimal gypsum dosage is of great significance to CBSC's durability.

These curves also reveal that the UCS of the CBSC is significantly influenced by the initial water content of the soft clay and the curing duration. Under the same G/C ratio, the UCS decreases with increasing initial water content. Taking samples with a G/C ratio of 15% for example, when the initial water content increases from 50% to 70%, the strength of the CBSC decreases from 1.73 MPa to 1.53 MPa after 60 d of curing. Additionally, when the G/C ratio increases from 0% to the threshold values, the strengths of the CBSC with initial water contents of 50% and 70% increase by 0.49 MPa and 0.61 MPa, respectively. This demonstrates that gypsum, an industrial waste but used here as a special additive, is more effective in increasing the strength of soft clays with relatively higher initial water contents, primarily because the higher porosity in the soft clays with higher water contents can accommodate the growth and volumetric expansion of ettringite resulting from the reactions between the added gypsum and calcium aluminate, leading to the beneficial densification caused by the pore-filling and volumetric expansion along with the ettringite growth.

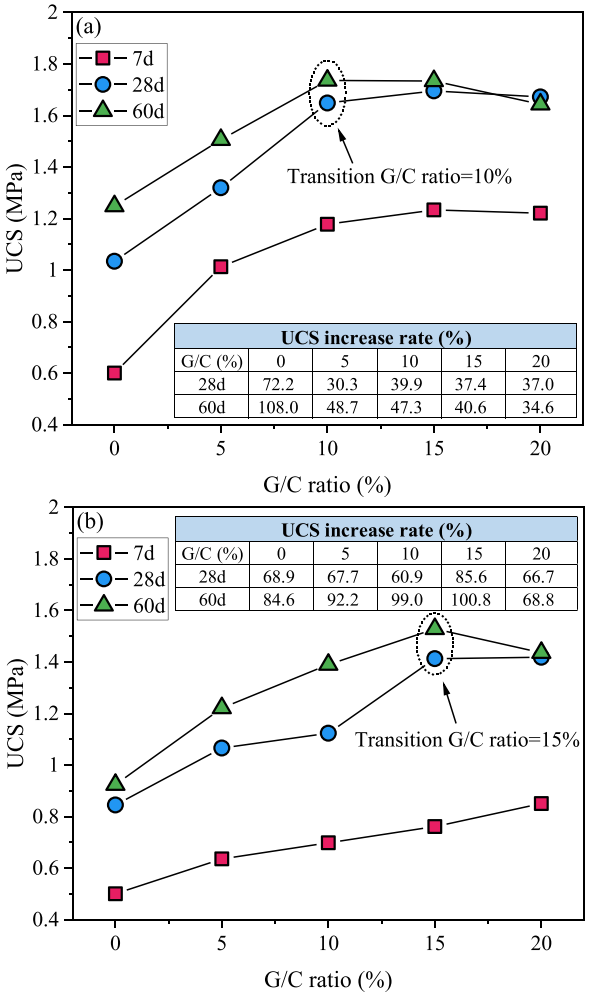

Fig. 4. UCS of the CBSC with varying G/C ratios at different initial water contents and curing durations: (a) 50% initial water content, and (b) 70% initial water content.

It should be noted that the aforementioned thresholds of the G/C ratio are only applicable to the studied specific type of clay. Apart from the initial water content, the thresholds of the G/C ratio in the CBSC are also conditioned and affected by the composition and physicochemical properties of the treated clay, such as its mineralogy, porewater pH value, soluble salts, and organic matter content, among others (Deng et al., 2020).

Fig. 5 shows the effect of the G/C ratio on the stiffness of the CBSC. Especially, linear regression is performed to find the best-fitted curves to the experimental data, and corresponding mathematical equations with the coefficient of determination R^2 are summarized in Table 4 to help analyze the dependence of the CBSC's deformation behavior (i.e. stiffness or modulus) on the G/C ratio. It can be seen that the ε_f of the CBSC decreases with increasing G/C ratio, but the E_{50} increases, irrespective of the curing periods and initial water content. For example, for the 60 d-cured CBSC sample with an initial water content of 70%, when the G/C ratio increases from 0% to 20%, the ε_f decreases by 1.02%, while the E_{50} increases by 98.2 MPa. This is different from the growth mode of the UCS where a threshold of the G/C ratio exists to identify an optimal dosage of gypsum. Moreover, this further implies that the addition of gypsum can reduce the ductility but increase the brittleness of the CBSC. The pore-filling effect induced by the expansive ettringite particles from the reactions of gypsum and calcium aluminate is responsible for this behavior change. In addition, the cementitious binders-induced reduction in water content and pertinent increase in dry density also play positive roles in the enhancement of the strength and stiffness of the CBSC (Fig. 3).

3.2.3. UCS-ε_f and UCS-E_{50} relationships

As mentioned earlier, the change in the E_{50} is highly consistent with the development of UCS for the CBSC samples studied. As such, similar analyses can be conducted to correlate the UCS with the ε_f based on the obtained experimental data. As shown in Figs. 6 and 7, the quantitative relationships between the UCS and ε_f and between UCS and E_{50} are obtained.

Fig. 6 shows the unified UCS-ε_f curves of all the CBSC samples with different initial water contents and different gypsum contents. It can be seen that most ε_f values are distributed in the range of 1.49%–3.13%, and the ε_f tends to decrease with increasing UCS. Using the least-squares regression analysis, the experimental data of the UCS versus ε_f can be well fitted by a power function expressed by

$$UCS = 3.02\varepsilon_f^{-1.33} \left(R^2 = 0.88\right) \tag{3}$$

The fitting correlation coefficient, $R^2 = 0.88$, suggests that the derived power function may be used as a practically useful empirical formula to characterize the relationship between the ε_f and UCS of the CBSC. Increasing its strength can change the CBSC to be a less ductile material.

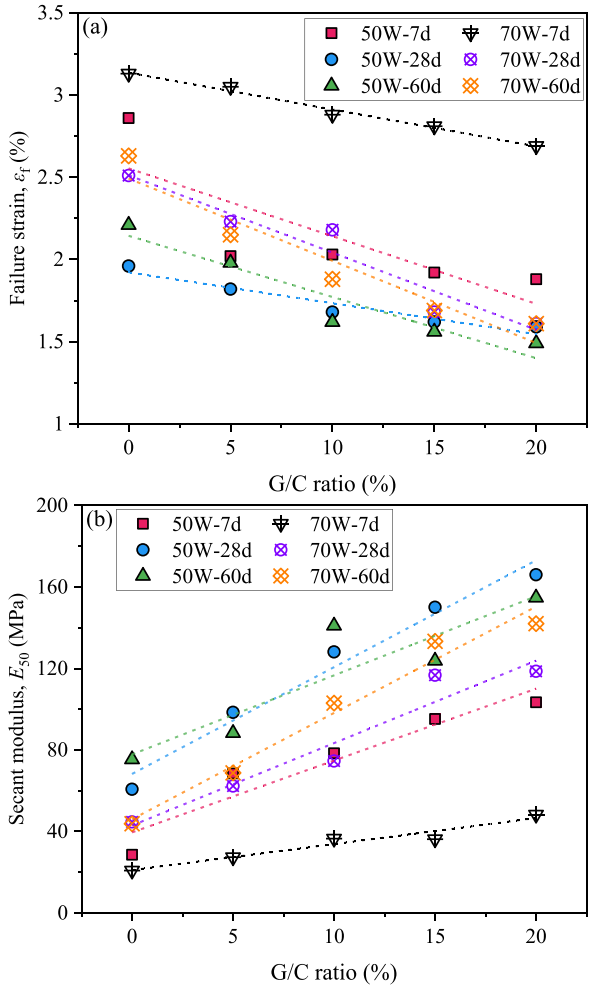

Fig. 5. Evolution of failure strain and modulus for samples with varying G/C ratio: (a) Failure strain ε_f, and (b) Secant modulus E_{50}.

The secant modulus, E_{50}, for all samples treated with different G/C ratios, is also plotted against the corresponding UCS in Fig. 7. The increase in the E_{50} is highly consistent with the increase in UCS, and the maximum E_{50} of 166 MPa is obtained for the samples with a G/C ratio of 20% and an initial water content of 50%. Lorenzo and Bergado (2006) indicated that the E_{50} has a linear correlation with the UCS, as expressed by

Table 4
Fitting equations of ε_f and E_{50}.

Sample ID	Fitting equation	R^2
50W-7d	$\varepsilon_f = 2.554-0.041(G/C)$	0.52
	$E_{50} = 39.56 + 3.526(G/C)$	0.88
50W-28d	$\varepsilon_f = 1.922-0.019(G/C)$	0.91
	$E_{50} = 68.24 + 5.242(G/C)$	0.96
50W-60d	$\varepsilon_f = 2.144-0.037(G/C)$	0.87
	$E_{50} = 77.81 + 3.882(G/C)$	0.75
70W-7d	$\varepsilon_f = 3.136-0.022(G/C)$	0.98
	$E_{50} = 21.08 + 1.276(G/C)$	0.92
70W-28d	$\varepsilon_f = 2.512-0.047(G/C)$	0.91
	$E_{50} = 42.94 + 4.044(G/C)$	0.91
70W-60d	$\varepsilon_f = 2.492-0.05(G/C)$	0.89
	$E_{50} = 45.99 + 5.219(G/C)$	0.96

Note: Sample ID notation such as 50W-60d represents all samples with 50% initial water content after 60 d of curing.

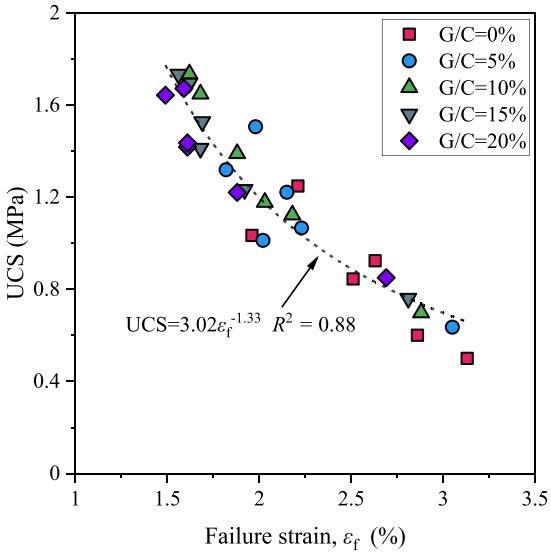

Fig. 6. Relationship between the unconfined compressive strength and failure strain.

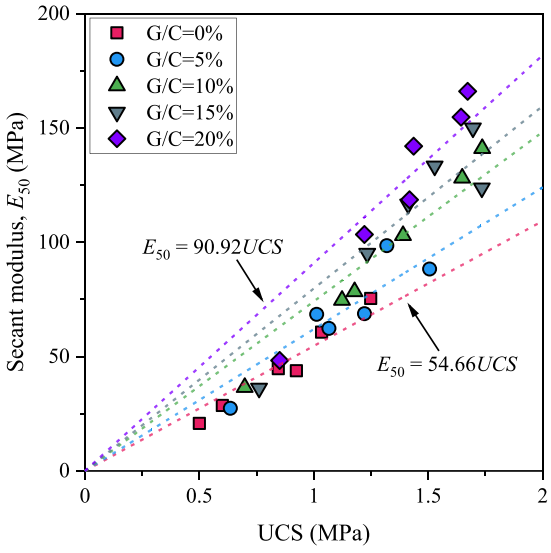

Fig. 7. Relationship between the UCS and secant modulus.

$$E_{50} = \eta UCS \tag{4}$$

where η is a dimensionless fitting parameter. Here the parameter η is obtained using the least-squares fitting, and the results are tabulated in Table 5. It is observed that there is a reasonably strong correlation (i.e. $R^2 > 0.82$) between the UCS and E_{50} with a linear equation for samples with different G/C ratios. From Table 5, it can be seen that the η varies in the range of 54.66–90.92, and increases with the G/C ratio. The underlying hypothesis is that, for the same strength improvement, the cementitious binders with a higher G/C ratio make the CBSC behave more brittle as compared with those with a lower G/C ratio. This phenomenon indicates that the gypsum content has a remarkable impact on not only the stress-strain relationships and strength characteristics (as summarized in Figs. 3 and 4), but also the UCS and E_{50} relationships. Therefore, the optimal G/C ratio deserves more attention in consideration of avoiding loading-induced cracking of the CBSC, especially when used as the base, subbase, or subgrade materials for highways, in particular for roads with high-intensity traffic.

Table 5
Comparison of relationships between UCS and E_{50}.

Material	Equation	R^2	Source
Cement-stabilized soil	$E_{50} = 130\ UCS$		Tang et al. (2000)
Cement-treated sediment	$E_{50} = 167.32\ UCS$	0.94	Zhu et al. (2005)
Cement-stabilized plastic soil	$E_{50} = 106.71\ UCS - 6.46$	0.95	Yilmaz and Ozaydin (2013)
Cement-based stabilized sediment	$E_{50} = 119.91\ UCS$	0.8	Wang et al. (2013)
CBSC	$E_{50} = 159\ UCS$		Zhang et al. (2014)
Cement-based stabilized sediment	$E_{50} = 81.79\ UCS$	>0.9	Wang et al. (2017)
CBSC (0G/C)	$E_{50} = 54.66\ UCS$	0.91	This study
CBSC (5G/C)	$E_{50} = 61.99\ UCS$	0.82	This study
CBSC (10G/C)	$E_{50} = 74.14\ UCS$	0.92	This study
CBSC (15G/C)	$E_{50} = 79.79\ UCS$	0.85	This study
CBSC (20G/C)	$E_{50} = 90.92\ UCS$	0.85	This study

Note: Notation such as 5G/C represents the sample with G/C ratio of 5%.

3.3. Microstructure

3.3.1. PSD

Fig. 8 presents the MIP results by plotting the cumulative and the differential mercury intrusion volumes per unit mass of soil against the entrance pore diameter of the CBSC treated with different G/C ratios (i.e. 0%, 15% and 20%) at varied curing periods (i.e. 7 d and 60 d). The cumulative intrusion volume for the sample without gypsum is 0.309 mL/g, but this value decreases to 0.253 mL/g and 0.261 mL/g for the samples treated with G/C ratios of 15% and 20%, respectively, indicating that the porosity of the one with G/C ratio of a 15% is the smallest or its solid packing density is the highest. The reason is most likely the pore-filling effect induced by the ettringite at suitable or optimal amounts, and this finding is consistent with the UCS analysis where a threshold of the G/C ratio exists, as discussed earlier. The PSD curves are also plotted in Fig. 8, in which the vertical axis is defined as $dv/d\log_{10}d$, where v is the volume of the intruded mercury at a given pressure increment, which is also the volume of pores with a diameter of d in 1 g dry soil. Also, there is a tendency that the main peak moves from the right (i.e. corresponding to larger pores) to left (i.e. corresponding to smaller pores) successively with increasing G/C ratio. This phenomenon is attributed to the prevailing effect of gypsum on the production of ettringite, which fills a large fraction of the pores that is previously filled with water in the soft clays with high water content.

The statistical deconvolution results are presented in Fig. 9, and the PSD curves mostly exhibit bimodal characteristics. However, interestingly, only one unimodal curve is observed for the sample treated at the threshold of the G/C ratio of 15%. As suggested by earlier researchers (Li and Zhang, 2009; Hattab et al., 2013), the dual peaks in the PSD curves represent the relatively smaller intra-aggregate and relatively larger inter-aggregate pores, respectively. Accordingly, gypsum seems more efficient than Portland cement or lime in accelerating the filling of inter-aggregate pores. Meanwhile, Chew et al. (2004) concluded that an increase in the fraction of smaller intra-aggregate pores is mainly attributed to the filling of relatively larger inter-aggregate pores by the C–S–H and ettringite, thus implying that the gypsum and calcium aluminate reactions lead to an increase in ettringite fraction and thereby a decrease in the fraction of relatively larger inter-aggregate pores, whilst accompanied by an increase in the fraction of intra-aggregate pores, conditioned by adding a suitable dosage of cementitious binders.

Table 6 summarizes the parameters obtained from the fitted PSD curves of the CBSC: a_1 and a_2, the volumetric fractions of the intra- and inter-aggregate pores, respectively; and μ_1 and μ_2, the mean diameters of the intra- and inter-aggregate pores, respectively. It reveals that when the G/C ratio increases from 0% to 15%, a_1 increases by 8.8% while μ_1 decreases by 70.4% for the 60 d-cured samples. Moreover, with the continuous increase in the gypsum content, the opposite trend is observed, and this is similar to the mechanical behavior. It is worth noting that the curing period also plays a pivotal role in the pore structure of the CBSC, since the morphology and quantity of ettringite and other C–S–H cementation agents between particles do shift significantly upon progressive reactions. For example, for the samples treated with a 15% G/C ratio, the fitted parameters show a considerable difference for

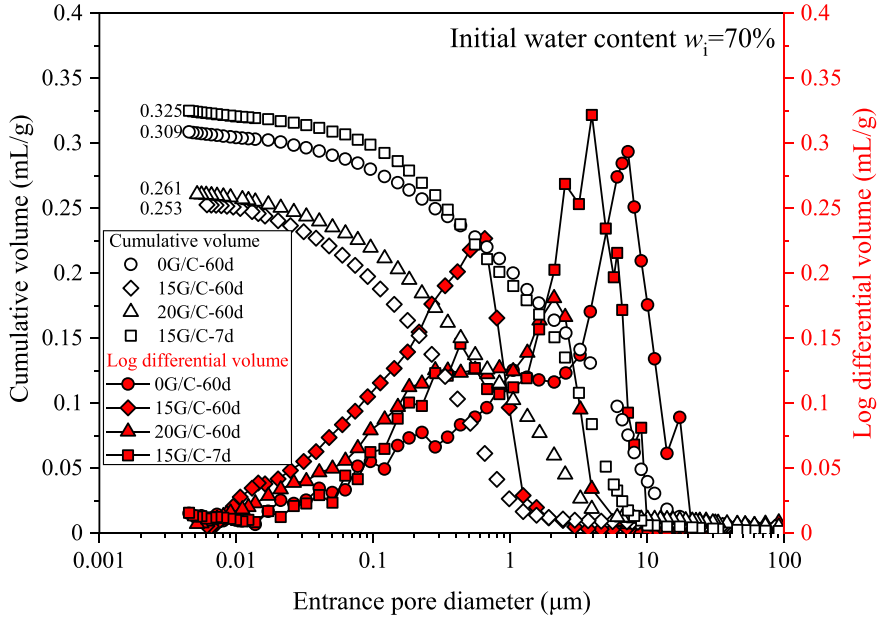

Fig. 8. Entrance pore diameter distribution curves of the CBSC at an initial water content of 70%.

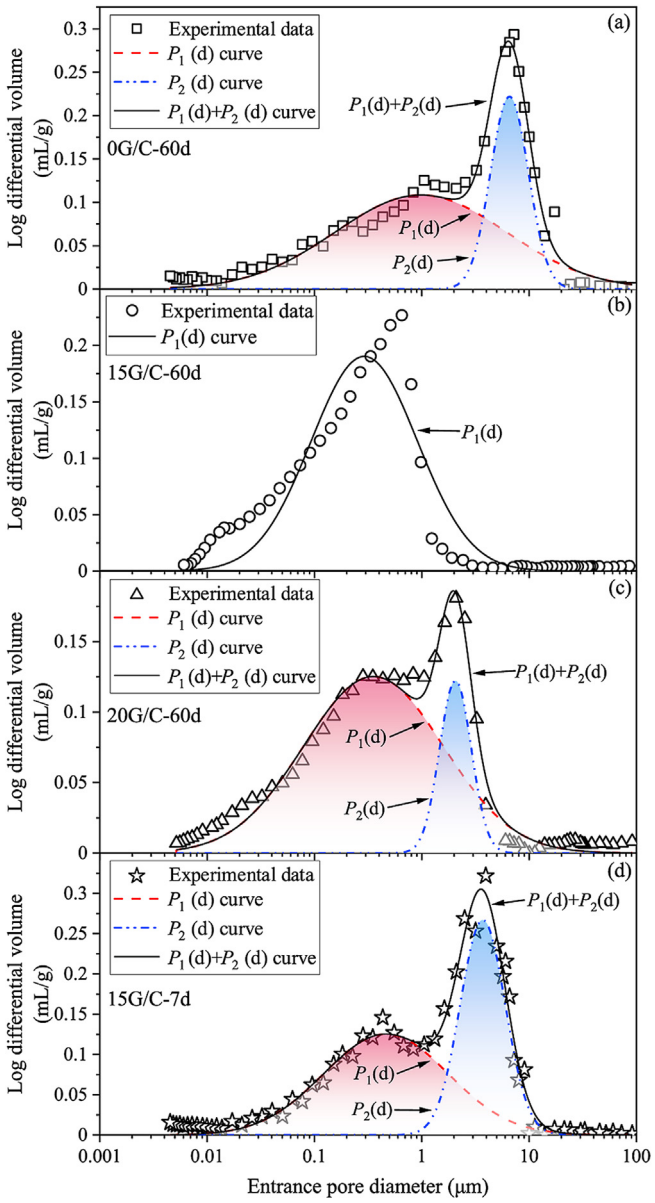

Fig. 9. Deconvolution of the PSD curves of the CBSC at an initial water content of 70%: (a) 0% G/C ratio after 60 d of curing, (b) 15% G/C ratio after 60 d of curing, (c) 20% G/C ratio after 60 d of curing, and (d) 15% G/C after 7 d of curing.

Table 6
Summary of the deconvolution results for the PSD curves of the CBSC.

Sample ID	n	a_1 (mL/g)	a_2 (mL/g)	μ_1 (μm)	μ_2 (μm)	σ_1	σ_2	R^2
0G/C-60d	2	0.217	0.098	0.98	6.57	0.798	0.177	0.97
15G/C-60d	1	0.236		0.29		0.495		0.87
20G/C-60d	2	0.204	0.045	0.35	2.06	0.65	0.148	0.97
15G/C-7d	2	0.182	0.141	0.46	3.7	0.581	0.21	0.97

Note: Sample ID notation such as 15G/C-60d represents the sample with 15% G/C ratio after 60 d of curing; n - number of peaks in the fitted PSD curves; σ_1, σ_2 - standard deviations.

the 7- and 60-d curing: the numbers of deconvoluted peaks are 2 and 1, a_1 values are 0.182 mL/g and 0.236 mL/g, and μ_1 values are 0.46 μm and 0.29 μm, respectively. These differences can be attributed to the time-dependent reaction between gypsum and calcium aluminate. In other words, the formation of ettringite and the resulting expansion is a kinetic, time-dependent process as compared with other hydration reactions (e.g. calcium silicates hydration in the clinker) and pozzolanic reactions (e.g. alkaline activation of silica and alumina, leading to the formation of C–S–H and C-A-H). It can thus be concluded that changes in the pore structure of the CBSC are manifested by not only the gypsum content but also the curing period.

3.3.2. *Microstructure imaging*

As manifested by the SEM images in Fig. 10, substantial amounts of the C–S–H gels are cross-attached to the ettringite surface, which increases the surface roughness and, therefore, strengthen the interfacial frictional force. As such, the CBSC's resistance to the displacement and rearrangement of particles at the ettringite-clay interface increases. In addition, Diamond (1996) observed that the growing ettringite crystals can penetrate the interlayer space of layered mica in concrete. As such, it can be speculated that the growing ettringite can function as bridging links within the solid skeleton matrix (i.e. including clay particles and other solid hydration/pozzolanic products) under the condition of an appropriate void ratio and gypsum concentration (Fig. 11). Such solid ettringite bridges can effectively impede the further development and growth of microcracks when the CBSC samples are subjected to overloading.

4. Discussion

4.1. *Mechanisms of gypsum-based stabilization*

Upon the mixing of the composite cementitious binders, including the clinker, metakaolin and gypsum, with the soft clay and water, a series of physicochemical reactions takes place in the CBSC, such as hydration, ion exchange, carbonation and pozzolanic alkali activation. These reactions generate various primary and secondary newly formed products, such as the C–S–H, C-A-H, $Ca(OH)_2$, ettringite and $CaCO_3$, as illustrated schematically in Fig. 11. These hydration and reaction products not only enhance the cementation bonds among the CBSC soil particles and aggregates but also fill the voids within the CBSC, making the solid particle packing denser (Oluwatuyi and Ojuri, 2017; Oluwatuyi et al., 2018; Al-Alawi et al., 2020; Amrani et al., 2020; Wu et al., 2021). Although numerous complex, sometimes simultaneous, physical, mineralogical and chemical reactions take place in the CBSC, the composition of the Portland cement (i.e. clinker) used in the CBSC and other derived cementitious products (e.g. cement paste, mortar and concrete) is not yet altered in accordance. Hence, at present, increasing the cement dosage instead of adjusting the cement composition is the commonly accepted method to achieve better and optimal improvement in the strength of the CBSC, which is a fundamental deficiency in terms of engineering, economic and environmental perspectives.

In particular, as one of the constituents in Portland cement, gypsum plays a non-negligible role in the CBSC. Generally, gypsum itself does not have any cementitious properties. However, with the participation of clinker and metakaolin, it can react with calcium aluminate to form the acicular ettringite crystals (see Eq. (1)), which are approximately 1–2 μm and sometimes even up to 10 μm in length (Taylor, 1997). Given the fact that the soft clay is usually characterized by high porosity, an extremely high water content, and sometimes a high organic matter content, the formation of ettringite by the proper incorporation of gypsum can generate pore infills as well as the reinforcement or cementation effect in the CBSC (Fig. 11), providing higher strength and stiffness to the treated

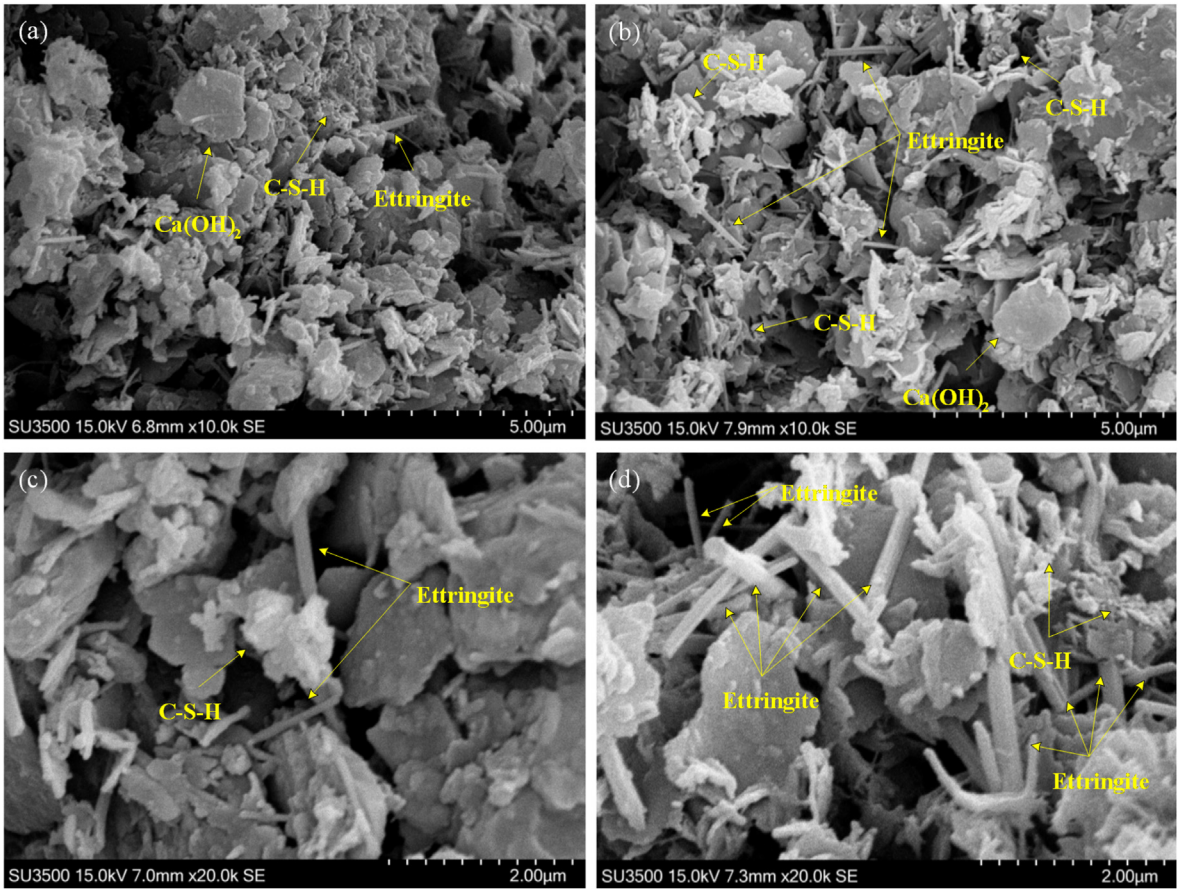

Fig. 10. SEM images of the CBSC after curing for 60 d: (a) 5G/C–70W, (b) 20G/C–70W, (c) 10G/C–50W, and (d) 20G/C–50W.

CBSC. The progressive growth of ettringite can fill the voids existing in the treated soft clay (Fig. 11), leading to an increase in its dry density (Fig. 2) and thereby making the matrix denser. The reinforcement or cementation effect of ettringite originates from the mechanical interfacial interactions of the acicular ettringite and reticulated C–S–H, including interfacial adhesion and friction, to form a reinforced, inter-penetrating network structure that interlinks and bonds clay particles (Fig. 11).

Despite the superior properties mentioned above, gypsum does not always play positive, beneficial roles in the improvement of mechanical behavior of soft clays and other soils with dense packing of solid particles, and its threshold dosage usually needs to be determined experimentally, beyond which further addition of gypsum should not be expected to bring higher or better benefits and may sometimes even compromise the improvement resulting from the low dosage (Fig. 4). The reason is most likely that the continuous, excessive growth of ettringite can generate significant internal stresses due to the volumetric expansion of ettringite. In particular, when confronted with excessive ettringite growth after prolonged curing, the internal expansion stress, equivalent to tensile stress, may reach or exceed the tensile strength of the CBSC and hence local tensile failure occurs inevitably, thus significantly degrading the samples. In this regard, it is hypothesized that the contribution of ettringite to strength improvement is more pronounced for CBSC with relatively higher water contents, equivalent to inherently higher porosities. For example, for the specific studied soft marine clay, the optimal G/C ratio is 10% for the samples with an initial water content of 50% whilst 15% for the initial water content of 70% (Fig. 4).

4.2. Research limitations

This study only investigated the role of gypsum on the mechanical behavior of CBSC. The OPC contains five main constituents, including tricalcium silicate (C_3S), dicalcium silicate (C_2S), tricalcium aluminate (C_3A), tetracalcium alumino ferrite (C_4AF), and the sulfate phase (often gypsum, CSH_2) (Taylor, 1997). After hydration and reactions, each constituent generates specific hydration products (e.g. C–S–H, C-A-H and ettringite) with different characteristics, including (but not limited to) particle size and particle morphology, thereby resulting in different microfilling and bonding efficiencies. In particular, when it is adopted to stabilize soft clays with various mineral compositions, the complexity becomes more pronounced due to the coupling effect between the hydration products and clay minerals (Latifi et al., 2015). Therefore, characterization of the interactions between pure clay minerals (e.g. kaolinite, montmorillonite, illite, chlorite, palygorskite and sepiolite) and individual cement constituents (e.g. C_3S, C_2S, C_3A, C_4AF and gypsum) still warrants further effort, which is essential to deepen the recognition of strength generation in the CBSC and establish more rational design guides for this kind of heterogeneous natural soft materials.

It was noteworthy that the results were mainly derived under laboratory-scale conditions, and the in situ effectiveness and applicability still require further exploration. Especially, for CBSC that serves in a seawater environment, a major detrimental effect, sulfate attack, may occur in the presence of sulfate ions, thereby yielding additional expansion due to the continuous formation of ettringite (Yi et al., 2014). Therefore, in engineering practice, it is

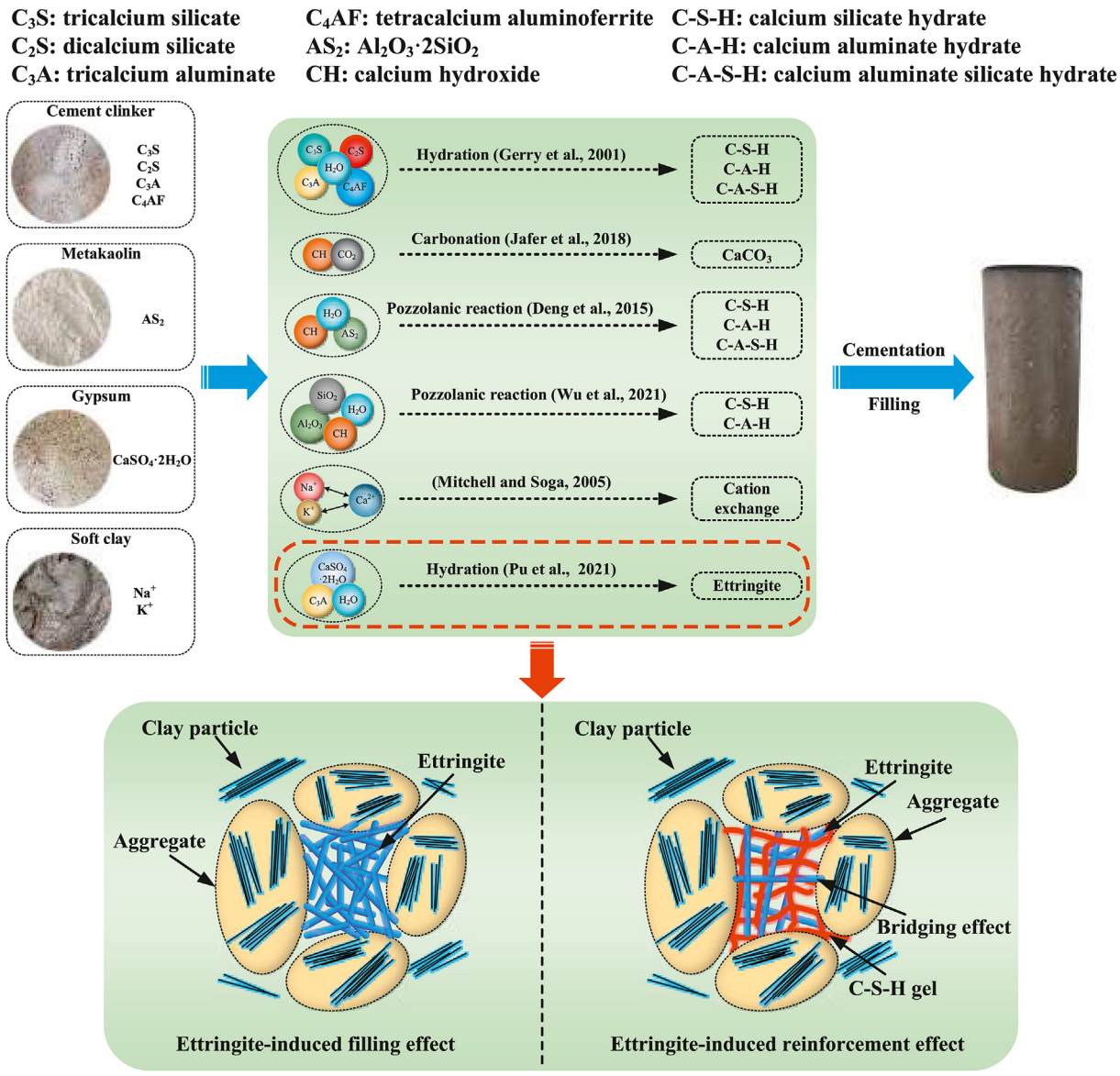

Fig. 11. Mechanisms of cement-based stabilization of clays, particularly showing the beneficial roles of ettringite.

necessary to consider the host clay's sulfate content when determining the optimal content of gypsum in CBSC.

5. Conclusions

In this paper, adjusting the gypsum fraction in the OPC's constituents has been proposed as a cost-effective and environmentally friendly technology for the treatment and improvement of very soft clays with very high initial water contents as well as the beneficial reuse of industrial gypsum waste. The mechanical performance of the CBSC treated with different G/C ratios was investigated using a series of laboratory tests, including density and water content measurements, unconfined compression, porosimetry, and microstructure observation and imaging. According to the analyses of results, the following conclusions can be drawn:

(1) After curing for 60 d, when the G/C ratio increases from 0% to 20%, the final water content of the treated soft clays decreases by 7.8% and 11.2% for clays with 50% and 70% initial water contents, while the final dry density increases by 10.5% and 12.3% for clays with 50% and 70% initial water contents, respectively. This indicates that the influence of gypsum content on the final water content and dry density is significant.

(2) The UCS of the CBSC tends to increase with the G/C ratio. The threshold of the G/C ratio is defined as the transition point beyond which further addition of gypsum has no further improvement in the strength, and such a threshold of the G/C ratio is highly dependent on the initial water content of the soft clay, i.e. 10% and 15% for clays with 50% and 70% initial water contents, respectively. At these thresholds of the G/C ratio, the UCS values for clays with 50% and 70% initial water contents are 1.74 MPa and 1.53 MPa after 60 d of curing, respectively. Moreover, an excessively high gypsum fraction can hinder the further improvement in the CBSC's strength. Generally, an increase in the G/C ratio leads to increased initial stiffness and brittleness of the CBSC.

(3) Microstructural investigations by MIP and SEM reveal that ettringite-induced filling and cementation are responsible for the improved mechanical performance of the CBSC. The hydration of gypsum leads to an increase in ettringite volume, and thus switches the relatively large inter-aggregate pores to relatively smaller intra-aggregate pores to some extent, resulting in a lower total porosity and finer pore sizes.
(4) The above beneficial role of gypsum is closely associated with the increase in the density of very soft clays, due to the formation and accompanied volumetric expansion of ettringite. However, such an effect may disappear in stiff clays or soils with dense solid packing. In addition, the host clay's sulfate content should be taken into account in engineering practice to ensure CBSC's long-term durability.

Declaration of competing interest

The authors declare that they have no known competing financial interests or personal relationships that could have appeared to influence the work reported in this paper.

Acknowledgments

This study was supported by the National Key R&D Program of China (Grant No. 2019YFC1806004) and National Natural Science Foundation of China (Grant Nos. 51878159 and 41572280).

References

Al-Alawi, H.S., Ganiyu, A.A., Badr, A., 2020. Stabilisation of Sohar's Sabkha soil using waste gypsum plasterboard. In: IOP Conference Series: Materials Science and Engineering, 849. IOP Publishing, 012028.
Amrani, M., Taha, Y., Kchikach, A., Benzaazoua, M., Hakkou, R., 2020. Phosphogypsum recycling: new horizons for a more sustainable road material application. J. Build. Eng. 30, 101267.
ASTM C150-21, 2021. Standard Specification for Portland Cement. ASTM International, West Conshohocken, PA, USA.
ASTM D854-14, 2014. Standard Test Methods for Specific Gravity of Soil Solids by Water Pycnometer. ASTM International, West Conshohocken, PA, USA.
ASTM D2166M-16, 2016. Standard Test Method for Unconfined Compressive Strength of Cohesive Soil. ASTM International, West Conshohocken, PA, USA.
ASTM D1632-17, 2017. Standard Practice for Making and Curing Soil-Cement Compression and Flexure Test Specimens in the Laboratory. ASTM International, West Conshohocken, PA, USA.
ASTM D2487-17, 2017. Standard Practice for Classification of Soils for Engineering Purposes (Unified Soil Classification System). ASTM International, West Conshohocken, PA, USA.
Ahmed, A., El Naggar, M.H., 2016. Swelling and geo-environmental properties of bentonite treated with recycled bassanite. Appl. Clay Sci. 121, 95–102.
BS EN197-1, 2011. Cement Composition, Specifications and Conformity Criteria for Common Cements. British Standards Institution, London, UK.
Chew, S.H., Kamruzzaman, A.H.M., Lee, F.H., 2004. Physicochemical and engineering behavior of cement treated clays. J. Geotech. Geoenviron. Eng. 130 (7), 696–706.
Deng, Y.F., Yue, X.B., Liu, S.Y., Chen, Y.G., Zhang, D.W., 2015. Hydraulic conductivity of cement-stabilized marine clay with metakaolin and its correlation with pore size distribution. Eng. Geol. 193, 146–152.
Deng, Y.F., Wu, J., Tan, Y.Z., Cui, Y.J., Tang, C.S., Zhou, A.N., 2020. Effects of microorganism within organic matter on the mechanical behaviour of solidified municipal dredged mud. Can. Geotech. J. 57 (12), 1832–1843.
Diamond, S., 1996. Delayed ettringite formation - processes and problems. Cement Concr. Compos. 18 (3), 205–215.
Du, Y.J., Jiang, N.J., Liu, S.Y., Jin, F., Singh, D.N., Puppala, A.J., 2014. Engineering properties and microstructural characteristics of cement-stabilized zinc-contaminated kaolin. Can. Geotech. J. 51 (3), 289–302.
Eyo, E., Ng'ambi, S., Abbey, S., 2020. Performance of clay stabilized by cementitious materials and inclusion of zeolite/alkaline metals-based additive. Transp. Geotech. 23, 100330.
Eyo, E., Abbey, S., Oti, J., Ng'ambi, S., Ganjian, E., Coakley, E., 2021. Microstructure and physical-mechanical characteristics of treated kaolin-bentonite mixture for application in compacted liner systems. Sustainability 13 (4), 1617.
Gerry, B., Paul, L., Leslie, S., 2011. Portland Cement, third ed. ICE Publishing, London, UK.
Gu, K., Chen, B., 2020. Loess stabilization using cement, waste phosphogypsum, fly ash and quicklime for self-compacting rammed earth construction. Construct. Build. Mater. 231, 117195.
Hattab, M., Hammad, T., Fleureau, J., Hicher, P., Mesri, G., 2013. Behaviour of a sensitive marine sediment: microstructural investigation. Geotechnique 63 (1), 71–84.
Horpibulsuk, S., Miura, N., Bergado, D.T., 2004. Undrained shear behavior of cement admixed clay at high water content. J. Geotech. Geoenviron. Eng. 130 (10), 1096–1105.
Justice, J.M., Kurtis, K.E., 2007. Influence of metakaolin surface area on properties of cement-based materials. J. Mater. Civ. Eng. 19 (9), 762–771.
Kim, H., Lee, S., Moon, H., 2007. Strength properties and durability aspects of high strength concrete using Korean metakaolin. Construct. Build. Mater. 21 (6), 1229–1237.
Latifi, N., Rashid, A.S.A., Siddiqua, S., Horpibulsuk, S., 2015. Micro-structural analysis of strength development in low- and high swelling clays stabilized with magnesium chloride solution-A green soil stabilizer. Appl. Clay Sci. 118, 195–206.
Lee, F.H., Lee, Y., Chew, S.H., Yong, K.Y., 2005. Strength and modulus of marine clay-cement mixes. J. Geotech. Geoenviron. Eng. 131 (2), 178–186.
Li, X., Zhang, L.M., 2009. Characterization of dual-structure pore-size distribution of soil. Can. Geotech. J. 46 (2), 129–141.
Liu, L., Zhou, A.N., Deng, Y.F., Cui, Y.J., Yu, Z., Yu, C., 2019. Strength performance of cement/slag-based stabilized soft clays. Construct. Build. Mater. 211, 909–918.
Lorenzo, G.A., Bergado, D.T., 2006. Fundamental characteristics of cement-admixed clay in deep mixing. J. Mater. Civ. Eng. 18 (2), 161–174.
Luo, S.M., Lu, Y.H., Wu, Y.K., Song, J.L., DeGroot, D.J., Jin, Y., Zhang, G.P., 2020. Cross-scale characterization of the elasticity of shales: statistical nanoindentation and data analytics. J. Mech. Phys. Solid. 140, 103945.
Oluwatuyi, O.E., Ojuri, O.O., 2017. Environmental performance of lime-rice husk ash stabilized lateritic soil contaminated with lead or naphthalene. Geotech. Geol. Eng. 35 (6), 2947–2964.
Oluwatuyi, O.E., Adeola, B.O., Alhassan, E.A., Nnochiri, E.S., Modupe, A.E., Elemile, O.O., Obayanju, T., Akerele, G., 2018. Ameliorating effect of milled eggshell on cement stabilized lateritic soil for highway construction. Case Stud. Constr. Mater. 9, e00191.
Oluwatuyi, O.E., Ashaka, E.C., Ojuri, O.O., 2019. Cement stabilization treatment of lead and naphthalene contaminated lateritic soils. J. Environ. Eng. Landsc. Manag. 27 (1), 41–48.
Oluwatuyi, O.E., Ojuri, O.O., Khoshghalb, A., 2020. Cement-lime stabilization of crude oil contaminated kaolin clay. J. Rock Mech. Geotech. Eng. 12 (1), 160–167.
Pu, S.Y., Zhu, Z.D., Huo, W.W., 2021. Evaluation of engineering properties and environmental effect of recycled gypsum stabilized soil in geotechnical engineering: a comprehensive review. Resour. Conserv. Recycl. 174, 105780.
Puppala, A.J., Griffin, J.A., Hoyos, L.R., Chomtid, S., 2004. Studies on sulfate-resistant cement stabilization methods to address sulfate-induced soil heave. J. Geotech. Geoenviron. Eng. 130 (4), 391–402.
Suarez, S., Roca, X., Gasso, S., 2016. Product-specific life cycle assessment of recycled gypsum as a replacement for natural gypsum in ordinary Portland cement: application to the Spanish context. J. Clean. Prod. 117, 150–159.
Tang, S.W., Zhu, H.G., Li, Z.J., Chen, E., Shao, H.Y., 2015. Hydration stage identification and phase transformation of calcium sulfoaluminate cement at early age. Construct. Build. Mater. 75, 11–18.
Tang, Y.X., Liu, H.L., Zhu, W., 2000. Study on engineering properties of cement-stabilized soil. Chin. J. Geotech. Eng. 22 (5), 549–554.
Taylor, H.F., 1997. Cement Chemistry, second ed. Academic Press, London, UK.
Tremblay, H., Leroueil, S., Locat, J., 2001. Mechanical improvement and vertical yield stress prediction of clayey soils from eastern Canada treated with lime or cement. Can. Geotech. J. 38 (3), 567–579.
Tsuchida, T., Tang, Y.X., 2015. Estimation of compressive strength of cement-treated marine clays with different initial water contents. Soils Found. 55 (2), 359–374.
Wang, D.X., Abriak, N.E., Zentar, R., 2013. Strength and deformation properties of Dunkirk marine sediments solidified with cement, lime and fly ash. Eng. Geol. 166, 90–99.
Wang, D.X., Zentar, R., Abriak, N.E., 2017. Temperature-accelerated strength development in stabilized marine soils as road construction materials. J. Mater. Civ. Eng. 29 (5), 4016281.
Wu, J., Liu, Q.W., Deng, Y.F., Yu, X.B., Feng, Q., Yan, C., 2019a. Expansive soil modified by waste steel slag and its application in subbase layer of highways. Soils Found. 59 (4), 955–965.
Wu, J., Deng, Y.F., Zheng, X.P., Cui, Y.J., Zhao, Z.P., Chen, Y.G., Zha, F.S., 2019b. Hydraulic conductivity and strength of foamed cement-stabilized marine clay. Construct. Build. Mater. 222, 688–698.
Wu, J., Liu, L., Deng, Y.F., Zhang, G.P., Zhou, A.N., Wang, Q., 2021. Distinguishing the effects of cementation versus density on the mechanical behavior of cement-based stabilized clays. Construct. Build. Mater. 271, 121571.
Wu, Z.L., Deng, Y.F., Liu, S.Y., Liu, Q.W., Chen, Y.G., Zha, F.S., 2016. Strength and microstructure evolution of compacted soils modified by admixtures of cement and metakaolin. Appl. Clay Sci. 127, 44–51.
Xu, L.L., Wu, K., Li, N., Zhou, X.Y., Wang, P.M., 2017. Utilization of flue gas desulfurization gypsum for producing calcium sulfoaluminate cement. J. Clean. Prod. 161, 803–811.
Yi, Y.L., Li, C., Liu, S.Y., Al-Tabbaa, A., 2014. Resistance of MgO-GGBS and CS-GGBS stabilised marine soft clays to sodium sulfate attack. Geotechnique 64 (8), 673–679.
Yilmaz, I., Civelekoglu, B., 2009. Gypsum: an additive for stabilization of swelling clay soils. Appl. Clay Sci. 44 (1), 166–172.

Yilmaz, Y., Ozaydin, V., 2013. Compaction and shear strength characteristics of colemanite ore waste modified active belite cement stabilized high plasticity soils. Eng. Geol. 155, 45–53.
Zhang, M., Zhao, M.X., Zhang, G.P., Nowak, P., Coen, A., Tao, M.J., 2015. Calcium-free geopolymer as a stabilizer for sulfate-rich soils. Appl. Clay Sci. 108, 199–207.
Zhang, T.W., Yue, X.B., Deng, Y.F., Zhang, D.W., Liu, S.Y., 2014. Mechanical behaviour and micro-structure of cement-stabilised marine clay with a metakaolin agent. Construct. Build. Mater. 73, 51–57.
Zhao, M., Guo, W., Chen, L.Y., Wang, S.Y., 2019. Experiment on the frost resistance of modified phospho gypsum: a case used to improve baozhong railway subgrade loess. J. Mt. Sci. 16 (12), 2920–2930.
Zhu, W., Zhang, C.L., Gao, Y.F., Fan, Z.P., 2005. Fundamental mechanical properties of solidified dredged marine sediment. J. Zhejiang Univ. 39 (10), 1561–1565.

Yongfeng Deng obtained his BSc degree from Chongqing Jiaotong University, China, in 1999, and his MSc and PhD degrees from Southeast University, China in 2002 and 2005, respectively. He is now a professor at School of transportation, Southeast University since 2014. His research interest includes (1) soil behaviours under evolution of geological environment, (2) geotechnical testing method and underground structure, and (3) ground improvement and soil modification. Until now, Prof. Deng has led many national and provincial research projects, including four National Natural Science Foundations and a National Key R&D Program of China. He has published more than 50 SCI papers as first or corresponding author.